Peer-reviewed version available at *Materials* **2020**, *13*, 1601; doi:10.3390/ma13071601

Article

Collaborative Optimization on Density and Surface Roughness of 316L Stainless Steel in Selective Laser Melting

Yong Deng[1,2], Zhongfa Mao[1,3,*], Nan Yang[1], Xiaodong Niu[1,3], Xiangdong Lu[1]

[1] Intelligent Manufacturing Key Laboratory of Ministry of Education, Shantou University, Shantou 515063, China; dengyong@stu.edu.cn (Y.D.); zfmao@stu.edu.cn (Z.M.); nyang@stu.edu.cn (N.Y.); xdniu@stu.edu.cn (X.N.); 15xdlu@stu.edu.cn (X.L.)
[2] Digital Technology Research and Application Center, Shantou Polytechnic, Shantou 515078, China
[3] Shantou Ray-Bonus Additive Manufacture Research Institute, Shantou 515063, China
* Correspondence: zfmao@stu.edu.cn(Z.M.) ; xdniu@stu.edu.cn (X.N.); Tel.: +86-0754-8650-2153

Abstract: Although the concept of additive manufacturing has been proposed for several decades, momentum of selective laser melting (SLM) is finally starting to build. In SLM, density and surface roughness, as the important quality indexes of SLMed parts, are dependent on the processing parameters. However, there are few studies on their collaborative optimization in SLM to obtain high relative density and low surface roughness simultaneously in the previous literature. In this work, the response surface method was adopted to study the influences of different processing parameters (laser power, scanning speed and hatch space) on density and surface roughness of 316L stainless steel parts fabricated by SLM. The statistical relationship model between processing parameters and manufacturing quality is established. A multi-objective collaborative optimization strategy considering both density and surface roughness is proposed. The experimental results show that the main effects of processing parameters on the density and surface roughness are similar. It is noted that the effects of the laser power and scanning speed on the above objective quality show highly significant, while hatch space behaves an insignificant impact. Based on the above optimization, 316L stainless steel parts with excellent surface roughness and relative density can be obtained by SLM with optimized processing parameters.

Keywords: selective laser melting; 316L stainless steel; multi-objective optimization; relative density; surface roughness

1. Introduction

Selective Laser Melting (SLM) is an additive manufacturing (AM) technology based on high-power laser beam, which is the most widely used metal 3D printing technology [1]. SLM manufacturing is a rapid prototyping process, in which metal powder is melted and then solidified. Comparing with conventional manufacturing processes, SLM has many outstanding advantages, such as the capacity of manufacturing parts with complex structures, saving time and costs [1,2].

However, there are more than 130 parameters [3] of SLM which may have significant impacts on the forming properties (such as density and surface roughness) of the parts, including the diameter of the laser beam, laser power, scanning speed, hatch spacing, scanning strategy, layer thickness and so on [4-7]. Mumtaz [8], Song [9] and Dadbakhsh [10] investigated the effects of processing parameters including laser power, scanning speed on surface roughness, and revealed that higher laser power tended to reduce top surface roughness. Han et al. [11] studied the influence factors of the surface roughness in SLMed parts, and found that the surface roughness is mainly affected by the scanning speed and hatch spacing. Larimian et al. [12] investigated the effect of the scanning strategy on the density of 316L stainless steel SLMed parts and indicated that the higher scanning speeds had

Peer-reviewed version available at Materials 2020, 13, 1601; doi:10.3390/ma13071601

better densification. Ni et al. [13] investigated the density and mechanical properties of SLMed parts of processing parameters.

To obtain SLMed parts in higher quality, researches on the processing parameters optimization in SLM have been carried out. Wang et al. [14] proposed an orthogonal method to optimize the processing parameters and thus obtained a higher density. Song et al. [15] and Wang et al. [16] simulated the temperature distribution and optimized the laser scan speed by using finite element analysis (FEA) method. Li et al. [3] employed response surface methodology (RSM) to optimize the SLM parameters for better surface roughness.

The above researches mainly focus on the influences of single or multiple processing parameters on the surface roughness or density of SLMed parts, respectively. There are only few studies on the synergistic processing optimization on both roughness and density for 316L stainless steel by using RSM method in the literature.

In this study, the influence of laser power, scanning speed and hatch spacing on the density and surface roughness are studied. The relationship model of processing parameters and the forming quality is established. As a unique contribution, a multi-objective collaborative optimization strategy based on RSM is proposed for obtaining good surface roughness and density simultaneously.

2. Materials and Methods

2.1 Experimental materials

The raw material used in this study is 316L stainless steel powder (Hunan Farsoon High-Technology Co., Ltd, Hunan, China). This material, as one of the most commonly used stainless steel, has excellent corrosion resistance and high temperature resistance, and has been widely used in construction, petrochemical industry and food industry [1,17]. As shown in Figure 1, the morphology is almost spherical with some small satellite particles, which is favored to improve the flowability and distribution of the powder on the powder bed, and thus obtaining the good quality for the finished parts.

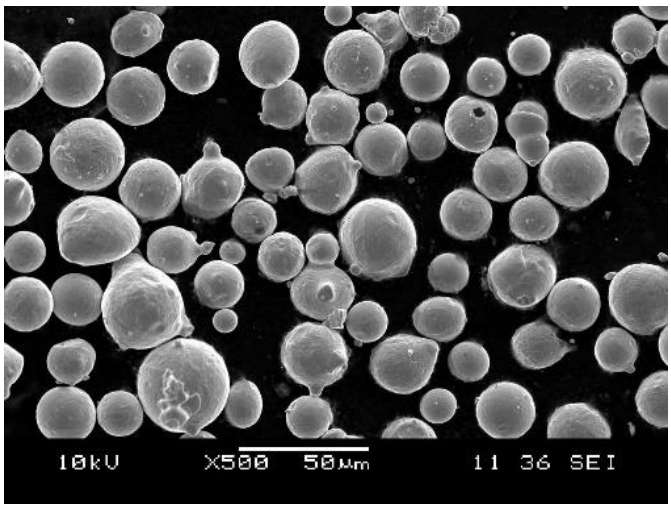

Figure 1. The morphology of the raw powder material

2.2 Experimental equipment

The employed SLM equipment in this study is an FS271M metal 3D printer (Hunan Farsoon High-Technology Co., Ltd, Hunan, China) and its corresponding specifications and parameters are shown in Table 1. The surface roughness (SR) was measured by TR200 roughness meter with an accuracy of 0.001μm (Beijing Jitai Scientific Instrument & Testing Equipment Co., Ltd) using a contact measurement method [18]. The relative density (RD) is expressed as the ratio between the measured density and the theoretical density. The measured density was acquired by BSM-220.4 electronic balance of (Shanghai Zhuojing Electronic Technology Co., Ltd) with Archimedes method [19]

Table 1. Machine specifications and parameters

Preprints (www.preprints.org) | NOT PEER-REVIEWED | Posted: 16 February 2020 doi:10.20944/preprints202002.0225.v1

Peer-reviewed version available at Materials 2020, 13, 1601; doi:10.3390/ma13071601

Property	Value
Machine	FS271M
Platform dimension (L×W×H)	275 mm×275 mm×320 mm
Laser type	Fiber laser
Laser diameter	70~200 μm
Maximum laser power	500 W
Maximum scan speed	15.2 m/s
Layer thickness	0.02~0.1 mm
Volume forming rate	20 cm^3/h

2.3 Experimental design and method

Response Surface Methodology (RSM) is a method of expressing the influences of multiple factors on the response by constructing a polynomial [20-22]. The objective is to find an optimal combination of factors which have an excellent response. The second-order polynomial response surface model [21] is shown in Equation (1).

$$Y = \beta_0 + \sum_{i=1}^{k} \beta_i x_i + \sum_{i=1}^{k} \beta_{ii} x_i^2 + \sum_{i<j}^{k} \beta_{ij} x_i x_j + \varepsilon \quad (1)$$

Where, Y represents the response, x_i represents the impact factor, β_i、β_{ii}、β_{ij} are undetermined coefficients, β_0 is the mean and ε is the error.

Central Composite Design (CCD), the most widely used method of RSM [22], is selected to design the experimental scheme. The influence factors in this experiment are laser power (P), scanning speed (V), and hatch spacing (S). The three parameters of each impact factor are corresponding to different levels. Each factor is coded at five levels, as shown in Table 2.

Table 2. Experimental processing parameters based on the response surface method

Influence factors	The levels of influence factors				
(Processing parameters)	-1.682	-1	0	1	1.682
Laser power (W)	150	180.4	225	269.6	300
Scanning speed (mm/s)	700	821.6	1000	1178.4	1300
Hatch spacing (μm)	60	72.2	80	107.8	120

3. Results

3.1 Main effects of processing parameters

The experimental scheme with 20 groups of experiments was designed in Minitab software, and experimental results were measured, as shown in Table 3. It can be seen that the optimal values of the density and the surface roughness in these samples can be obtained respectively when using the processing parameter sets (P, V, S) of NO.11 (225W, 700mm/s, 90μm) and NO.19 (225W, 1000mm/s, 90μm).

The main effects of processing parameters on RD and roughness are shown in Figure 2 and Figure 3. From Figure 2 and Figure 3, a great deal of information can be attained as follows: (1) With the laser power increasing in the range of 150-300 W, the RD of the SLMed parts first increases and then decreases. The maximum value occurs in P of near 270W. On the contrary, the SR first decreases and then increases. The minimum value appears at P of near 250 W. (2) Similarly, the RD first increases and then decreases with the increase of scanning speed from 700mm/s to1300mm/s, and reaches the maximum value at the V of near 840mm/s. However, the SR first decreases and then increases, the minimum value appears at the V of near 900 mm/s. (3) For different S, as the S increases from 60μm to 120μm, the RD increases firstly and then decreases, and the surface roughness decreases firstly and then increases. Their corresponding maximum/minimum values both occur around the S of 90μm.

Table 3. Experimental design matrix and measured results of SLMed 316L stainless steel parts

Standard sequence	The processing parameters			Measured value	Calculated value	Measured value
	P (w)	V (mm/s)	S (μm)	Density (g/cm³)	RD (%)	SR (μm)
1	180.4	821.6	72.2	7.845	98.31	11.57
2	269.6	821.6	72.2	7.870	98.62	10.38
3	180.4	1178.4	72.2	7.840	98.25	10.90
4	269.6	1178.4	72.2	7.871	98.63	10.35
5	180.4	821.6	107.8	7.869	98.61	10.25
6	269.6	821.6	107.8	7.863	98.53	8.47
7	180.4	1178.4	107.8	7.840	98.25	12.18
8	269.6	1178.4	107.8	7.851	98.38	10.73
9	150.0	1000.0	90.0	7.850	98.37	10.62
10	300.0	1000.0	90.0	7.877	98.71	8.35
11	**225.0**	**700.0**	**90.0**	7.879	**98.73**	8.11
12	225.0	1300.0	90.0	7.850	98.37	10.26
13	225.0	1000.0	60.0	7.855	98.43	11.73
14	225.0	1000.0	120.0	7.847	98.33	10.94
15	225.0	1000.0	90.0	7.872	98.65	8.73
16	225.0	1000.0	90.0	7.871	98.63	8.41
17	225.0	1000.0	90.0	7.870	98.62	8.06
18	225.0	1000.0	90.0	7.875	98.68	8.35
19	**225.0**	**1000.0**	**90.0**	7.877	98.71	**8.04**
20	225.0	1000.0	90.0	7.874	98.67	8.06

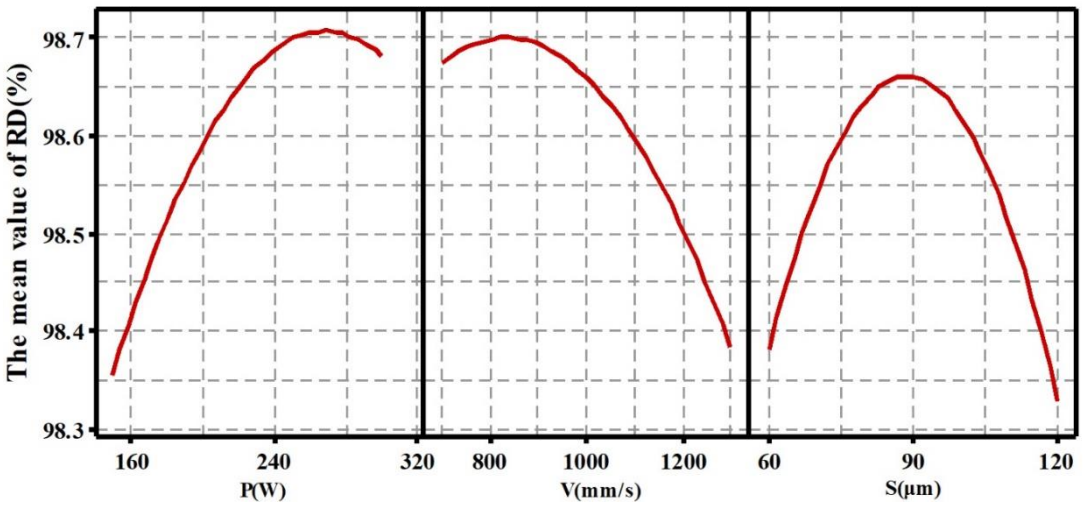

Figure 2. Main effects of processing parameters on RD

Peer-reviewed version available at Materials 2020, 13, 1601; doi:10.3390/ma13071601

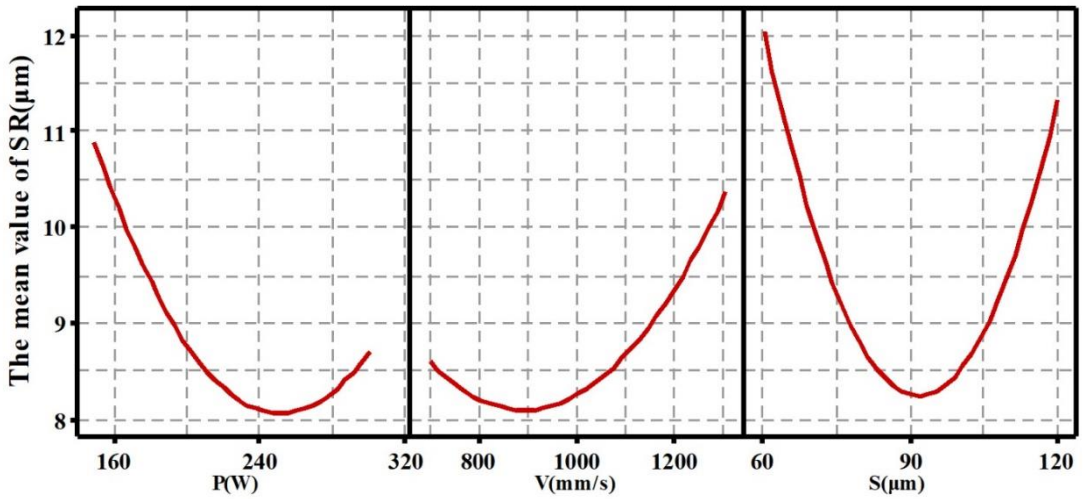

Figure 3. Main effects of processing parameters on SR

In order to better compare the effects of processing parameters on SR, some samples in Table 3 are chosen to observe their morphologies, as shown in Figure 4. It is noted that Figure 4(b, e, h) came from the identical sample with NO.17 in Table 3. Under the premise of keeping the other processing parameters as constant, surface morphologies of samples (NO. 9, 17, 10) with different P (150W, 225W, 300W) are shown in Figure 4(a-c). In Figure 4(a), when the P is 150W, a nodulizing phenomenon on the surface of the sample is obvious and unevenly distributed. When the laser power increases to 225W in Figure 4(b), a clear scaly feature can be observed, and homogeneous molten pool tracks contribute the excellent SR of 8.06μm. However, with the increase of the P, surface quality (Figure 4(c)) is worsened again. These features are consistent with main effect of P (Figure 3).

For different V (700mm/s，1000mm/s，1300mm/s)，surface morphologies of samples (NO. 11, 17, 12) are shown in Figure 4(d-f). It is interesting that there are few changes in surface morphology with the V increasing from 700mm/s to 1000mm/s, but it begins to dramatically worsen as the V further increase. When the V increases to 1300mm/s in Figure 4(f), the nodulizing phenomenon becomes obvious and some unmelted zones on the surface of sample are clearly visible. These features directly contribute to the deterioration of the surface quality, and simultaneously leads to the obvious reduction of the RD.

For different S (60μm, 90μm, 120μm), surface morphologies of samples (NO. 13, 17, 14) are shown in Figure 4(g-i). When S is 60μm, the uneven morphology (Figure 4(g)) on the single track can be clearly seen, confirming the unstable phenomenon of molten pool. As S increases to 90μm, the morphology becomes smoother and more uniform, as shown in Figure 4(h). However, When S further increases to 120μm, a large area of unmelted zones and serious nodulizing on the surface occurs again, proving that the laser energy is not enough to melt the powder.

Preprints (www.preprints.org) | NOT PEER-REVIEWED | Posted: 16 February 2020 doi:10.20944/preprints202002.0225.v1

Peer-reviewed version available at Materials 2020, 13, 1601; doi:10.3390/ma13071601

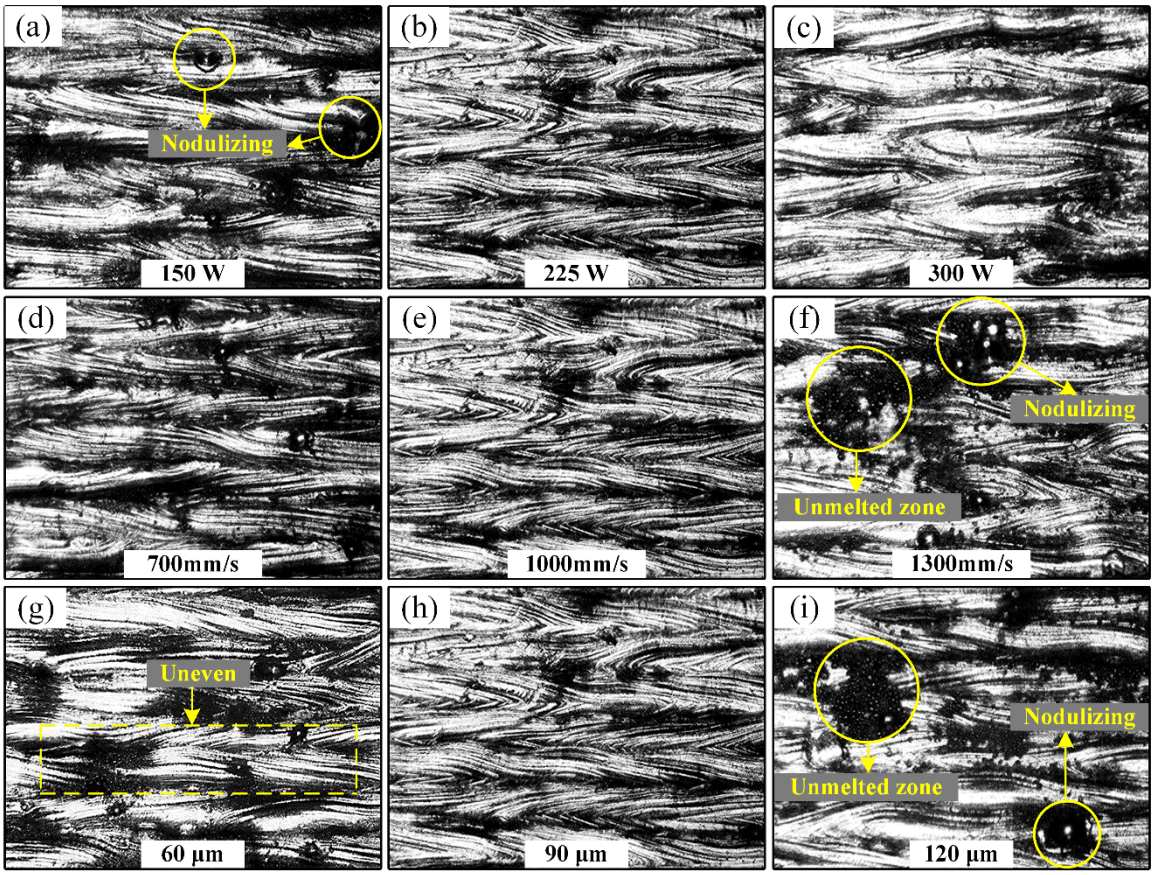

Figure 4. Surface morphologies of parts with different P of (a) 150W, (b) 225W and (c) 300W, and different V of (d) 700mm/s, (e) 1000mm/s and (f) 1300mm/s, and different S of (g) 60μm, (h) 90μm and (i) 120μm).

3.2 Analysis of variance

Based on measured datum (Table 3), analysis of variance (ANOVA) is carried out and the quadratic response surface models for RD and SR can be built using software Minitab. These models reflect the mathematical relationships between RD/SR and processing parameters respectively, as presented in the Equations (2) and (3).

$$RD = 82.91 - 0.1292P - 0.04473V - 0.8233S + 0.000268P^2 + 0.000013V^2 + 0.003733S^2 + 0.000015P * V - 0.000234P * S + 0.000192V * S \quad (2)$$

$$SR = 7.2433 + 0.001421P + 0.000236V + 0.007889S - 0.000002P^2 - 0.000000V^2 - 0.000026S^2 + 0.000000P * V - 0.000008P * S - 0.000001V * S \quad (3)$$

The results of ANOVA for RD and SR have been given in Table 4. F test is used to judge the significances of impact factors. For the linear effects in Table 4, it is found that the processing parameters have same significance of influences on the RD and the SR. The P-values of P and V are both less than 0.01, which indicates that their influences both on the RD and the SR are highly significant. The P-value of S is less than 0.25 and greater than 0.05, revealing that it has a weak influence. As for two-factor interaction effects, there are some differences between the RD and the SR. For the RD, P*V with the P-value (0.036) behaves a significant effect. What's more, P-values of P*S, V*S are both less than 0.01, proving that they have highly significant effects on the RD. However, for the SR, only V*S with the P-value (0.001) presents a significant effect. In addition, it can be seen in Table 4 that the models fit the experimental data well with the R^2 values of 96.65% and 96.54%, respectively. The corresponding prediction values R^2 are 80.26% and 79.77%, meaning that the models can effectively predict the RD and SR of parts.

Peer-reviewed version available at Materials 2020, 13, 1601; doi:10.3390/ma13071601

Table 4. Analysis of variance results for RD and SR

Source	DOF	Sum of squares		Covariance		The *F* value		*P* values	
		RD	SR	RD	SR	RD	SR	RD	SR
model	9	0.003299	37.2735	0.000367	4.1415	32.07	30.96	0.000	0.000
linear	3	0.001495	9.9677	0.000498	3.3226	43.59	24.84	0.000	0.000
P	1	0.000829	5.6546	0.000829	5.6546	72.54	42.27	0.000	0.000
V	1	0.000644	3.6997	0.000644	3.6997	56.33	27.66	0.000	0.000
S	1	0.000022	0.6134	0.000022	0.6134	1.90	4.59	0.198	0.058
Square	3	0.001258	23.9198	0.000419	7.9733	36.70	59.61	0.000	0.000
P^2	1	0.000229	4.0849	0.000229	4.0849	20.01	30.54	0.001	0.000
V^2	1	0.000190	2.6390	0.000190	2.6390	16.61	19.73	0.002	0.001
S^2	1	0.001022	20.3294	0.001022	20.3294	89.40	151.9	0.000	0.000
Two-factor interaction	3	0.000546	3.3859	0.000182	1.1286	15.93	8.44	0.000	0.004
P*V	1	0.000067	0.1193	0.000067	0.1193	5.89	0.89	0.036	0.367
P*S	1	0.000315	0.2764	0.000315	0.2764	27.56	2.07	0.000	0.181
V*S	1	0.000164	2.9902	0.000164	2.9902	14.33	22.35	0.004	0.001
Error	10	0.000114	1.3376	0.000011	0.1338				
Lack of Fit	5	0.000079	0.9595	0.000016	0.1919	2.28	2.54	0.193	0.165
Pure error	5	0.000035	0.3781	0.000007	0.0756				
Total	19	0.003413	38.6111						

Summary of the model

The standard deviation		Determination factor R^2		R^2 (Calibration)		R^2 (Prediction)	
RD	SR	RD	SR	RD	SR	RD	SR
0.0033807	0.365734	96.65%	96.54%	93.64%	93.42%	80.26%	79.77%

With an aim at obtaining the maximum RD and minimum SR simultaneously, multi-objective optimization considering both RD and SR were carried out according to the measured results. The optimization result is shown in Figure 5. Apparently, the composite optimal value can be obtained when the processing parameter set (P, V, S) is (259.1W, 900mm/s, 86.7μm), meaning that the RD of 98.72% and the SR of 8.04μm can reach to the relative optimal values simultaneously. Here, it is interesting that the S of 86.7μm is not the optimal value in the curve for the SR.

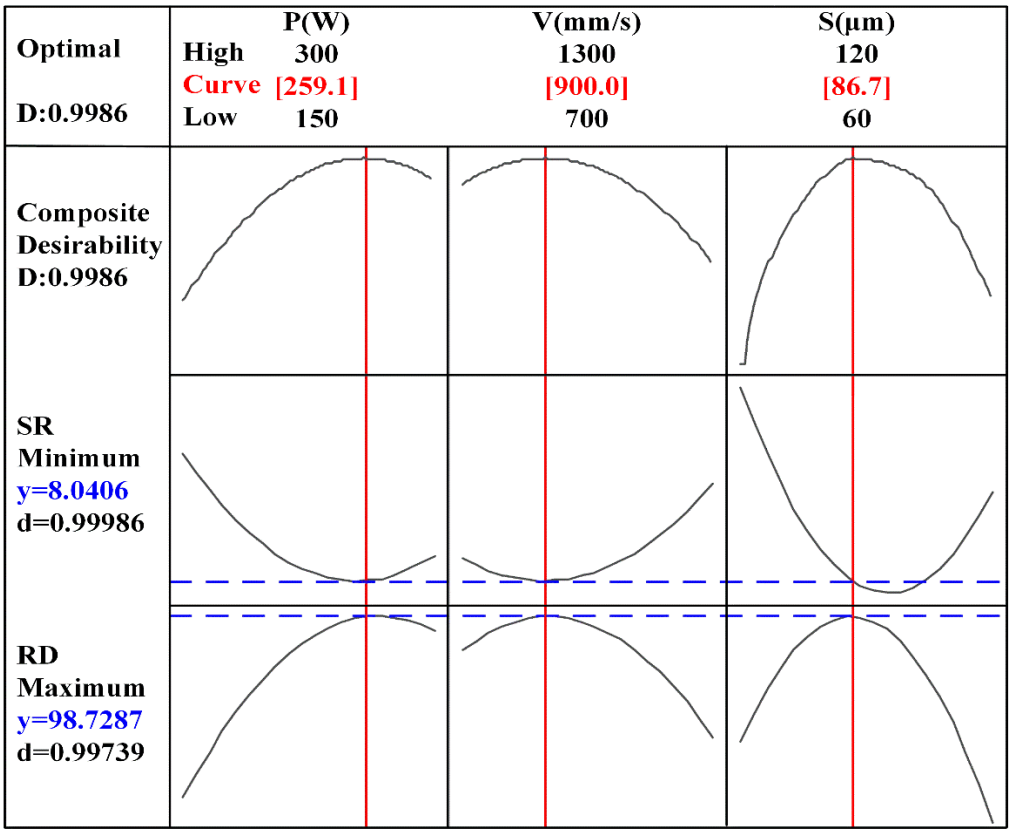

Figure 5. Multi-objective optimization plot for minimize SR and maximize RD

4. Discussion

The effects of processing parameters on RD are revealed. For single factor, both P and V have significant effects on the RD of parts, but that of S is weaker. The P almost has a positive correlation with the RD, which means that the higher P is, the higher RD will be. When P is too low, the metal powder cannot obtain enough energy to be melted completely, easily causing the nodulizing phenomenon and thus reducing the RD of the parts. In the defined range of V, a lower V is more conducive to obtain good RD for parts. This phenomenon can be explained as the increase in energy density caused by a lower V. Furthermore, too large or too small S are both bad for RD. If S is too large, the powder between adjacent molten paths is not completely melted, which causes inner porosity and bad RD of parts. If S is too small, there are major overlapping zones between adjacent single-tracks, leading to a large amounts of laser energy consumption through thermal conduction of consolidated materials instead of the powder, and causing an uneven temperature field and an unstable molten pool (Figure 4(g)). For interaction between two factors, it is found that the interaction effects of P*S and V*S are more significant than that of P*V. Therefore, it can be concluded that P and V should be adjusted first in the process of parameter optimization, and then S.

The effects of processing parameters on SR are also illuminated. P and V also have highly significant impacts on the SR of parts, while S has less impact. The results are close to the previous studies about RD resulting, because the surface quality of each layer directly affect the inner porosity of sample. The interaction effects of SR, P*V and P*S have very weak influences on SR, which can be explained as the decisive effect of the P. Changes of V and S don't affect the significance of P on SR. However, the effect of V*S on SR is highly significant, which is due to that S value depend on the influence of V on the single-track width.

When the composite desirability reaches the optimal value, not all parameters are optimal for RD and SR. This phenomenon is attributed to the interaction between processing parameters and compromise between optimization objectives.

5. Conclusions

This paper mainly involves the multi-objective optimization containing the RD and the SR of 316L stainless steel in SLM using RSM. The influences of processing parameters on the RD and the SR are investigated and discussed. The following conclusions can be drawn:

1. For the main effects of single factor, the influences of different processing parameters on the RD and the SR of 316L stainless steel are similar. The effects of P and V on RD and SR of parts are highly significant, but that of S is weak.
2. For interaction effects between two factors, there are some differences between the RD and the SR. All of the interaction influences containing P*V, P*S, V*S on the RD behave significantly, while on the SR only the V*S has a significant influence.
3. Based on the RSM and the ANOVA, the mathematical relationship model between the RD/SR and processing parameters have been built and can be used to effectively predict the processing parameters set or the target response.
4. According to multi-objective optimization, optimal processing parameters set with (P, V, S) of (259.1W, 900mm/s, 86.7μm) has been obtained, and thus resultant high RD of 98.7% and excellent SR of 8.04μm can be achieved simultaneously, which is in favor to further improve fatigue properties of SLMed 316L stainless steel products.

Author Contributions: Zhongfa Mao, Xiaodong Niu conceived and designed the experiments; Yong Deng, Zhongfa Mao performed the experiments and analyzed the data; Yong Deng wrote the paper; Zhongfa Mao, Nan Yang and Xiangdong Lu reviewed the paper; Yong Deng, Zhongfa Mao and Xiaodong Niu acquired funding for the work.

Funding: This research was funded by the Science and Technology Planning Project of Guangdong Province (Grant 2017A050501061), Scientific Research Foundation of Shantou University (Grant NTF18020), and Scientific Research Foundation of Shantou Polytechnic (Grant SZK2018Q02).

Acknowledgments: The authors would like to thank Bing Chen, Xuefen Xie of Shantou Ray-Bonus Additive Manufacture Research Institute and Adnan Khan of Shantou University for the assistance in the additive manufacturing and other helps.

Conflicts of Interest: The authors declare no competing interests.

References

1. Yap, C.Y.; Chua, C.K.; Dong, Z.L.; Liu, Z.H.; Zhang, D.Q.; Loh, L.E.; Sing, S.L. Review of selective laser melting: Materials and applications. *Applied Physics Reviews*. **2015**, *2*, 041101. [CrossRef]
2. Thijs, L.; Verhaeghe, F.; Craeghs, T.; Humbeeck, J.V.; Kruth, J.P. A study of the micro structural evolution during selective laser melting of ti-6al-4v. *Acta Mater*. **2010**, *58*, 3303–3312. [CrossRef]
3. Li, Z.H.; Kucukkoc, I.; Zhang, D.Z.; Liu, F. Optimising the process parameters of selective laser melting for the fabrication of Ti6Al4V alloy. *Rapid Prototyping Journal*. **2018**, *24*, 150-159. [CrossRef]
4. Badrossamay, M.; Childs, T.H.C. Further studies in selective laser melting of stainless and tool steel powders. *International Journal of Machine Tools & Manufacture*. **2007**,*47*, 779–784. [CrossRef]
5. Meier, C.; Weissbach, R.; Weinberg, J.; Wall, W.A.; Hart, A.J. Critical influences of particle size and adhesion on the powder layer uniformity in metal additive manufacturing. *Journal of Materials Processing Tech*. **2019**, *266*, 484–501. [CrossRef]
6. Xue, G.; Ke, L.D.; Zhu, H.H.; Liao, H.L.; Zhu, J.J.; Zeng, X.Y. Influence of processing parameters on selective laser melted SiCp/AlSi10Mg composites: Densification, microstructure and mechanical properties. *Materials Science & Engineering A*. **2019**, *764*, 138155. [CrossRef]
7. Majeed, A.; Ahmed, A.; Salam, A.; Sheikh, M.Z. Surface quality improvement by parameters analysis, optimization and heat treatment of AlSi10Mg parts manufactured by SLM additive manufacturing. *International Journal of Lightweight Materials and Manufacture*. **2019**, *2*, 288-295. [CrossRef]
8. Mumtaz, K.; Hopkinson, N. Top surface and side roughness of Inconel 625 parts processed using selective laser melting. *Rapid Prototyping Journal*. **2009**, *15*, 96-103. [CrossRef]

9. Song, B.; Dong, S.J.; Zhang, B.C.; Liao, H.L.; Coddet, C. The Effects of processing parameters on microstructure and mechanical property of selective laser melted Ti6Al4V. *Materials & Design*. **2012**, *35*, 120-125. [CrossRef]
10. Dadbakhsh, S.; Hao, L.; Jerrard, P.G.E.; Zhang, D.Z. Experimental study on selective laser melting behaviour and processing Windows of the in situ reacted Al/Fe2O3 powder mixture. *Powder Technology*. **2012**, *231*, 112–121. [CrossRef]
11. Han, X.; Zhu, H.; Nie, X.; Wang, G.; Zeng, X. Investigation on Selective Laser Melting AlSi10Mg Cellular Lattice Strut: Molten Pool Morphology, Surface Roughness and Dimensional Accuracy. *Materials*, **2018**, *11*, 392. [CrossRef]
12. Larimian, T.; Kannan, M.; Grzesiak, D.; AlMangour, B.; Borkar, T. Effect of energy density and scanning strategy on densification, microstructure and mechanical properties of 316L stainless steel processed via selective laser melting. *Materials Science & Engineering A*. **2020**, *770*, 138455. [CrossRef]
13. Ni, X.Q.; Kong, D.C.; Zhang, L.; Dong, C.F.; Song, J.; Wu, W.H. Effect of Process Parameters on the Mechanical Properties of Hastelloy X Alloy Fabricated by Selective Laser Melting. *Journal of Materials Engineering and Performance*. **2019**, *28*, 5533-5540. [CrossRef]
14. Wang, J.J.; Wu, W.J.; Jing, W.; Tan, X.P.; Bi, G.J.; Tor, S.B.; Leong, K.F.; Chua, C.K.; Liu, E. Improvement of densification and microstructure of ASTM A131 EH36 steel samples additively manufactured via selective laser melting with varying laser scanning speed and hatch spacing. *Materials Science & Engineering A*. **2019**, *746*, 300–313. [CrossRef]
15. Song, B.; Dong, S.J.; Liao, H.L.; Coddet, C. Process parameter selection for selective laser melting of Ti6Al4V based on temperature distribution simulation and experimental sintering. *The International Journal of Advanced Manufacturing Technology*. **2012**, *61*, 967-974. [CrossRef]
16. Wang, D. Song, C.H.; Yang, Y.Q.; Bai, Y.C. Investigation of crystal growth mechanism during selective laser melting and mechanical property characterization of 316L stainless steel parts. *Materials and Design*. **2016**, *100*, 291–299. [CrossRef]
17. Kong, D.C.; Dong, C.F.; Ni, X.Q.; Zhang, L.; Luo, H.; Li, R.X.; Wang, L.; Man, C.; Li, X.G. The passivity of selective laser melted 316L stainless steel. *Applied Surface Science*. **2020**, *504*, 144495. [CrossRef]
18. Jeong, H.S.; Ko, Y.C.; Kim, H.J. Effects of a stylus on the surface roughness determination in a contact method for paper and paperboard. *Nordic Pulp & Paper Research Journal*. **2019**, *34*, 442–452. [CrossRef]
19. Bai, S.G.; Perevoshchikova, N.; Sha, Y.; Wu. X.H. The Effects of Selective Laser Melting Process Parameters on Relative Density of the AlSi10Mg Parts and Suitable Procedures of the Archimedes Method. *Applied Sciences*. **2019**, *9*, 583. [CrossRef]
20. Liu, Y.; Zhang, J.; Pang, Z.C.; Wu, W.H. Investigation into the influence of laser energy input on selective laser melted thin-walled parts by response surface method. *Optics and Lasers in Engineering*. **2018**, *103*, 34–45. [CrossRef]
21. Yalçınkaya, Ö.; Bayhan, G.M. Modelling and optimization of average travel time for a metro line by simulation and response surface methodology. *European Journal of Operational Research*. **2009**, *196*, 225-233. [CrossRef]
22. Ding, E.; Cao, C.; Hua, H.Q.; Chen, Y.X. Lu, X.L. Application of central composite design to the optimization of fly ash-based geopolymers. *Construction and Building Materials*. **2020**, 230, 116960. [CrossRef]